

Estimation of High Velocities in Synthetic-Aperture Imaging—Part I: Theory

Jørgen Arendt Jensen^{ID}, Fellow, IEEE

Abstract—This paper describes a new pulse sequence design and estimation approach, which can increase the maximum detectable velocity in synthetic-aperture (SA) velocity imaging. In SA, N spherical or plane waves are emitted, and the sequence is repeated continuously. The N emissions are combined to form a high-resolution image (HRI). Correlation of HRIs is employed to estimate velocity, and the combination of N emissions lowers the effective pulse repetition frequency by N . Interleaving emission sequences can increase the effective pulse repetition frequency to the actual pulse repetition frequency, thereby increasing the maximum detectable velocity by a factor of N . This makes it possible to use longer sequences with better focusing properties. It can also increase the possible interrogation depth for vessels with large velocities. A new cross-correlation vector flow estimator is also presented, which can further increase the maximum detectable velocity by a factor of 3. It is based on transverse oscillation (TO), a preprocessing stage, and cross-correlation of signals beamformed orthogonal to the ultrasound propagation direction. The estimator is self-calibrating without estimating the lateral TO wavelength. This paper develops the theory behind the two methods. The performance is demonstrated in the accompanying paper for convex and phased array probes connected to the synthetic aperture real-time ultrasound system scanner for parabolic flow for both conventional and SA imaging.

Index Terms—Synthetic aperture, ultrasound imaging, velocity estimation.

I. INTRODUCTION

SYNTHETIC aperture (SA) velocity estimation was introduced in 2001 [1], [2]. Here, a repeated sequence of diverging emissions was used for reconstructing a continuous imaging sequence usable for velocity and vector velocity estimation. This resulted in highly accurate velocity estimates using directional beamforming [3] with relative standard deviations (SDs) down to 0.36% and very fast *in vivo* velocity images [2]. Only 24 emissions were used for imaging the carotid artery potentially yielding frame rates up to 10 kHz at a pulse repetition frequency f_{prf} of 24 kHz. Such continuous sequences can also be used with plane wave imaging, and the possibility of infinite observation times has been used to estimate very slow flow in the brain [4], [5] and to derive functional brain activity images. The main possibilities and advantages have been demonstrated by a number of research groups and are described in review papers [6]–[8].

Manuscript received July 22, 2018; accepted March 15, 2019. Date of publication March 20, 2019; date of current version June 5, 2019.

The author is with the Center for Fast Ultrasound Imaging, Department of Health Technology, Technical University of Denmark, 2800 Kongens Lyngby, Denmark (e-mail: jaje@elektro.dtu.dk).

Digital Object Identifier 10.1109/TUFFC.2019.2906384

There is, however, one disadvantage of SA as imaging sequences with a number of emissions have to be acquired to attain a high resolution and low sidelobes. The effective pulse repetition frequency $f_{\text{prf,eff}}$ is the emissions pulse repetition frequency f_{prf} divided by the emissions sequence length N , i.e., $f_{\text{prf,eff}} = f_{\text{prf}}/N$. The highest velocity detectable is directly proportional to $f_{\text{prf,eff}}$ and is, therefore, reduced by a factor N , which can lead to erroneous estimates for large velocities in the major arteries or in the heart. The solution is often to employ a very high f_{prf} , which generates massive amounts of data, precludes the investigation of deep vessels, and often creates probe temperature problems and limitations on the emitted fields.

Several factors influence the resolution limit and contrast for images, which also affects the velocity range possible to estimate. The resolution is determined by the F-number of the system, which is determined by the width of the aperture or rather the number of elements combined in reception, and the spread of the emissions in either angle for plane wave emissions or space for spherical emissions. Having a high number of emissions and receiving elements yields a good contrast and resolution as demonstrated in [9] for plane waves and in [10] for spherical waves. A long sequence will, however, reduce the effective $f_{\text{prf,eff}}$, and the effective frame rate of fully independent images is also reduced by a factor of N . In velocity imaging, the maximum detectable velocity is usually proportional to $\lambda f_{\text{prf}}/4$ for phase estimation methods before aliasing takes place [11], where λ is the wavelength. The maximum detectable velocity is, thus, also reduced by N , and obtaining both a high contrast for separating out adjacent vessels and a high-velocity range seems unbreakable in SA velocity imaging. A choice must, therefore, be made between looking at low-velocity flow in small vessels with a long sequence or having a shorter sequence for estimating fast flow as described in [12]. One approach to break the aliasing limit is to use cross-correlation methods [13]–[15] rather than the autocorrelation method [16] limited to motions within $\pm\lambda/2$. The largest velocities are, however, still limited by rapid decorrelation of the data. An other approach is to use a staggered pulse repetition method for ultrafast imaging of high velocities [17], which is restricted to be used for antialiasing in phase shift estimators.

This paper describes two methods for increasing the aliasing limit to obtain both a high contrast using a long sequence and, at the same time, obtain a high aliasing limit. The first improvement is a new sequence design presented in Section II,

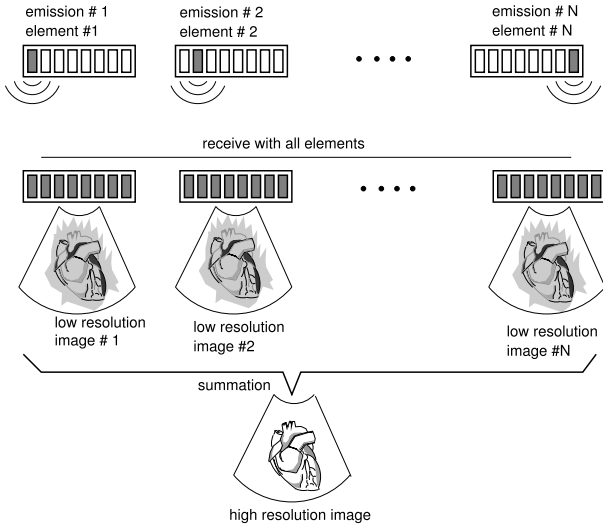


Fig. 1. Visualization of SAI. Spherical waves are emitted from a number of elements and the scattered signals are received on all the elements. An LRI is beamformed for each emission, and they are combined to yield an HRI with dynamic focusing in both transmit and receive (from [1]).

which maintains the highest possible $f_{\text{prf,eff}}$ equal to f_{prf} . This maintains a high peak detectable velocity with a reduced amount of data and makes interrogation of deep-lying vessels with a high peak velocity possible. The approach can be combined with any velocity estimator.

Second, a new estimator for the transverse oscillation (TO) approach is introduced [18]–[20], where cross-correlation is used. It can increase the detectable maximum velocity by a factor of 3 breaking the aliasing limit as demonstrated in the accompanying paper [21]. The lateral oscillation period can also be controlled dynamically during receive processing to increase or lower it depending on the flow velocities investigated. The estimator is derived in Section IV.

The accompanying paper [21] presents the Field II simulations [22], [23] and measurements using the synthetic aperture real-time ultrasound system (SARUS) experimental scanner [24] for revealing the performance of the methods.

II. SYNTHETIC-APERTURE FLOW IMAGING

SA imaging (SAI) insonifies a whole region of interest using spherical waves [6], [25] as illustrated in Fig. 1. A virtual source in the form of a spherical or plane wave is emitted. The spherical virtual source can have its origin behind or in front of the array and can use one or a number of elements combined [26]–[28]. A plane emission is defined by its tilt angle compared to the array, and all elements are usually needed in transmit. A low-resolution image (LRI), $L^{(1)}$, is beamformed after each emission, and this is dynamically focused during the receive beamforming based on the placement of the transmitted wave. A new wave is then emitted and the received data beamformed to yield $L^{(2)}$. The process is repeated for all N emissions in the sequence and all LRIs are combined to yield a high-resolution image (HRI), $H^{(N)}$, which is dynamically focused in both transmit and receive. The image is, thus, reconstructed over a number of emissions, and will, therefore, be affected by motion of the interrogated volume.

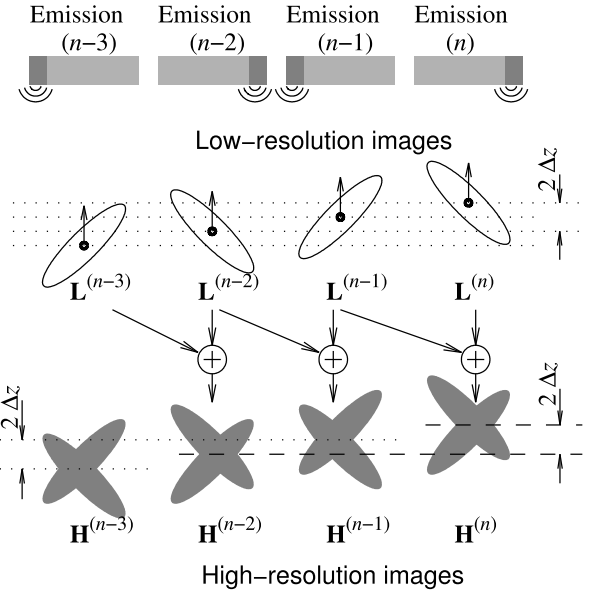


Fig. 2. SA sequence used for flow estimation using a two-emission sequence. Emitting virtual sources (top row). PSF for the LRIs (middle row). Resulting HRIs (bottom row). Similar HRIs can be correlated to estimate the velocity and the repeated sequence yields continuous data for the whole image (from [2]).

This is depicted in Fig. 2, which shows the point spread functions (PSFs) for the individual LRIs and the corresponding HRIs for a short two-emission sequence. The scatterer imaged is moving toward the probe by a distance of $\Delta z = v_z T_{\text{prf}} = v_z / f_{\text{prf}}$ between pulse emissions, where v_z is the axial velocity. The PSFs for the LRI are tilted toward the emitting source and are, therefore, different for each LRI in the sequence. The combined HRIs are also different, but it should be noted that the only difference for the same combination of LRIs $L^{(n-3)} + L^{(n-2)} = H^{(n-2)}$ and $L^{(n-1)} + L^{(n)} = H^{(n)}$ is the shift in position. These two HRIs can, therefore, be correlated to find the motion, and this is the key feature used in SA and plane wave flow imaging as was noticed and introduced by Nikolov and Jensen [1], [2] and Nikolov [25].

This ordering of the processing yields continuous data everywhere in the image, which makes it possible to track targets continuously and have very long echo canceling filters and averaging over as long time as the correlation functions are coherent [2], [29], [30]. The velocity can, thus, be found from any of the methods mentioned in [31]. Beamforming can also be performed in any direction and the flow can thus be tracked to minimize decorrelation effects from velocity gradients.

The standard method for SA flow imaging is shown in Fig. 3. A single HRI is created from the same colored block of LRIs and the correlation for finding velocities is between HRIs with a time difference of $T_{\text{prf}}N$. The averaging is across a number of HRI correlations to yield a low SD velocity estimate.

III. EMISSION SEQUENCE DESIGN

The largest velocity detectable for both spherical and plane wave synthetic aperture focusing (SAFs) $v_{z,\text{max}}$ is determined by the time interval between the two received signals that are

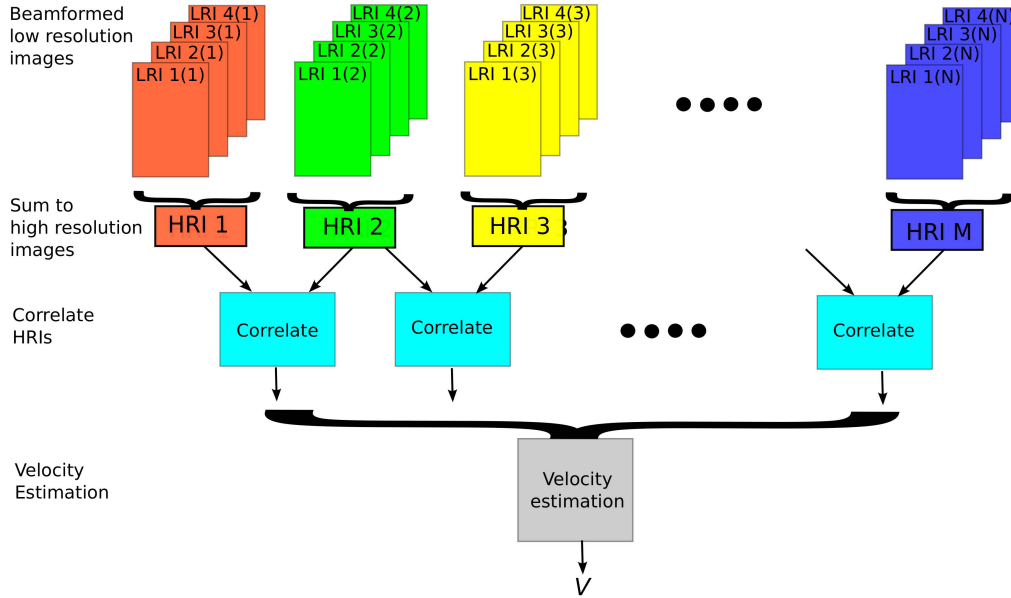


Fig. 3. Traditional SA sequence for velocity estimation. HRIs are created in blocks making the effective $f_{\text{prf,eff}}$ low. LRI 1(2) denotes LRI for emission 1 in high-resolution sequence 2 (first emission in the green block).

correlated and is for an autocorrelation (phase shift) estimator given as

$$v_{z,\text{max}} = \frac{\lambda}{4} f_{\text{prf,eff}}. \quad (1)$$

Keeping $f_{\text{prf,eff}}$ high, thus, ensures the highest detectable velocity. Ideally, the emissions for velocity estimation should be adjacent in time. This is precluded in a SAF system with a sequence length N so $f_{\text{prf,eff}} = f_{\text{prf}}/N$. The sequence should, therefore, be modified, so that HRIs are only one emission apart, at the same time as the sequence length N is maintained. This can be accomplished by interleaving two sequence. The normal sequence is given by

$$\begin{matrix} v_1^{(1)} & v_2^{(1)} & v_3^{(1)} & v_4^{(1)} & \dots, & v_N^{(1)}, & \dots \\ v_1^{(2)} & v_2^{(2)} & v_3^{(2)} & v_4^{(2)} & \dots, & v_N^{(2)} \end{matrix}$$

where $v_x^{(1)}$ is velocity emission sequence number 1 for spherical or plane wave source x . The source is here a virtual ultrasound source emission [27] or a plane wave in a given direction. Data are then beamformed for all emissions $v_1^{(1)}$ to $v_N^{(1)}$ to create high-resolution data $H^{(1)}$, and for emissions $v_1^{(2)}$ to $v_N^{(2)}$ to create high-resolution data $H^{(2)}$. The two high-resolution data sets are then correlated to estimate the velocity as shown in Fig. 3.

The suggested new sequence interleaves two sequences as shown in Fig. 4

$$v_1^{(1)} \quad v_1^{(2)} \quad v_2^{(1)} \quad v_2^{(2)} \quad \dots, \quad v_N^{(1)}, \quad v_N^{(2)}.$$

The two high-resolution data sets are beamformed, but $H^{(1)}$ and $H^{(2)}$ are now only one pulse emission apart, and this yields a correlation estimate with the highest possible maximum velocity for both the axial and lateral components. The correlation functions can be averaged over a number of

correlation pairs only limited by the acceleration of the flow. The length of averaging is limited by

$$aT < \sigma_v \quad (2)$$

where T is the averaging interval, a is acceleration, and σ_v is the SD on the estimate, which generally is dependent on T . This states that the correlation functions should be averaged as long as the peak position has not moved beyond the precision of the estimate. After this limit, the correlation will start to degrade.

This new sequence gives the optimal data for high-velocity estimation due to the shortest temporal distance between the high-resolution data. It breaks the link between sequence length N and maximum detectable velocity, and it can include long sequences with an optimal resolution and sidelobe level for detecting small vessels. The data sequence is continuous and can, therefore, be averaged over as long time as needed.

It can also be used for recursive SAI [32] as shown in Fig. 5. Here, a new HRI is created after each emission regardless of the imaging length for the fastest possible imaging. The notation $HRI\ 2(2)\ 3(2)\ 4(2)\ 1(4)$ indicates which set of emission is used. The first number is the emission (virtual source) from 1 to N in the sequence. The second number in parentheses is the sequence number used. Therefore, $3(2)$ is emission number 3 in the second sequence indicated by the light green color. It should be ensured that the same sequence of LRIs is used due to the distortion of the PSF, but after correlation, the functions are similar and can be averaged to increase precision.

The PSF will be affected by the velocity and, thus, the motion between emissions. This will result in a decorrelation of the LRIs, which affects the PSFs as described in [33]. This results in a reduction in SNR and higher sidelobes, which

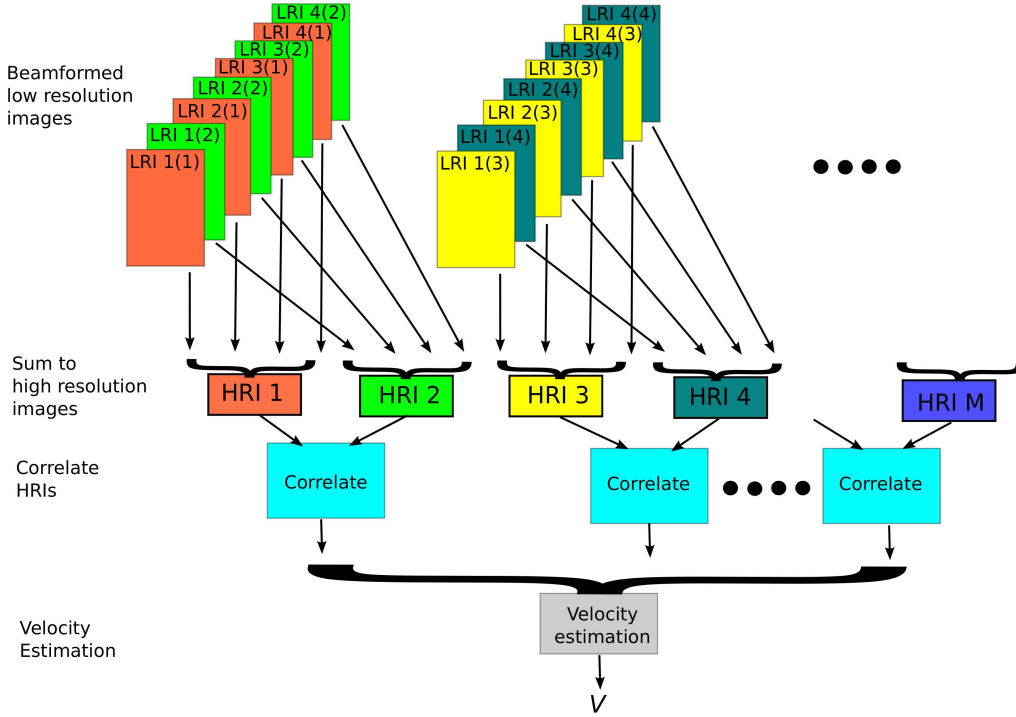


Fig. 4. Interleaved SA sequence where LRIs are repeated to minimize the distance between HRIs. The same colored LRIs are summed to yield one HRI. The effective $f_{prf,eff}$ is equal to the highest possible value due to the interleaving. Correlations in the blue boxes yield the same correlation function, which are then averaged to improve precision.

affects the velocity estimates. The length of the SA sequence will, therefore, be limited by the time over which the LRIs can be considered correlated. The correlation is affected by the interleaving as the sequence length is essentially doubled, which can lead to a drop in amplitude compared to a noninterleaved sequence. It has, however, been shown that the PSF can be fully recovered, if the velocity vector can be reliably estimated [33], [34], which is more likely for an interleaved sequence. The interleaving can also affect the variance of the estimates, as the length for acquiring data is doubled, thus reducing the averaging in half. The averaging time duration is restricted by the acceleration as given in (2), but often the estimates are more influenced by the echo canceling filter than limited by the averaging duration.

A. Echo Canceling

Echo canceling can be performed on the HRIs using the standard methods for removing stationary tissue signals [11]. It is benefited from having continuous data everywhere in the image [6], and a simple approach is to take the mean value across all HRIs and subtract this from the individual HRIs as used in the accompanying paper. Other more advanced techniques based on, e.g., decompositions [29], [35]–[39] can also be employed, when the continuous data are used as two interleaved high-resolution sequences, if equidistant sampling of the data is a requirement. Finite-impulse response (FIR) and IIR filters can thereby be used, and the continuous data remove limitations from the initial response of the filters. Singular value decomposition (SVD) and other decomposition

approaches can easily be adapted to handle the interleaving in one processing stage.

IV. DIRECTIONAL TRANSVERSE OSCILLATION USING CROSS-CORRELATION

The new sequence can be employed with any type of velocity estimation scheme based on correlation functions including autocorrelation [16], [40], cross-correlation [13], speckle tracking [15], directional beamforming [3], and TO [18]. TO introduces a lateral oscillation in the ultrasound field by employing a two-peak apodization waveform during receive beam formation. It can be optimized by focusing a directional signal transverse to the ultrasound propagation direction [directional transverse oscillation (DTO)] [41]. A Hilbert transform along this line is calculated to yield a complex signal usable for finding the sign of the transverse velocity. An autocorrelation estimator has been used to find the transverse velocity. This is limited to shifts less than a quarter lateral wavelength, and the maximum velocity is given by [11]

$$v_{x,max} = \frac{\lambda_x}{4} f_{prf} \tag{3}$$

where λ_x is the lateral wavelength. This restriction on maximum velocity coming from employment of phase shift estimation can be alleviated by using a cross-correlation estimator, where the maximum velocity is only limited by the decorrelation of the involved signals [11], [13]. This can be used on the directional signal but at beam-to-flow angles different from 90°, a significant oscillation from the axial motion will introduce a detrimental decorrelation. It can be seen from a model

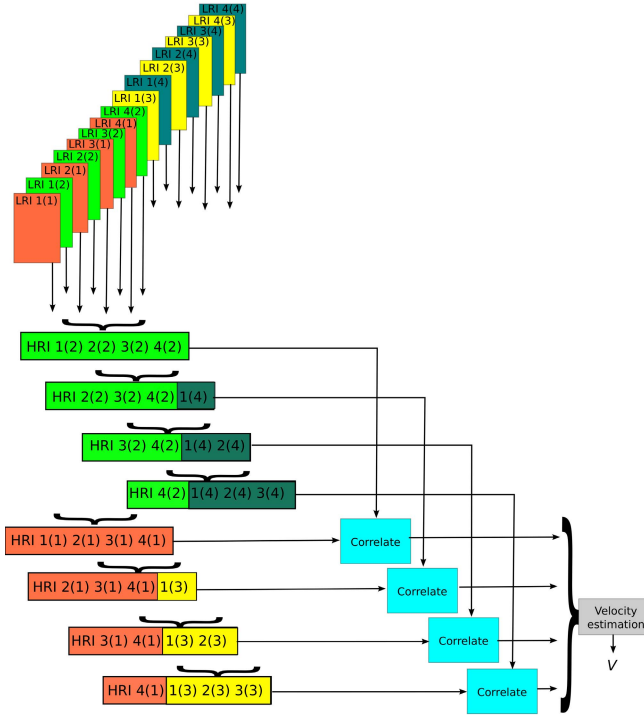


Fig. 5. Processing scheme for recursive SAF, where a new HRI is created after each pulse emission. *HRI 2(2) 3(2) 4(2) 1(4)* indicates which set of emission are used. The first number is the emission (virtual source) and the second number in parentheses is the sequence number used. Therefore, 3(2) is emission number 3 in the second sequence indicated by the light green color.

of the received signal. The received signal is $x(n, k, i)$ and its Hilbert transform along k is $y(n, k, i) = \mathcal{H}_k\{x(n, k, i)\}$, where \mathcal{H}_k denotes the Hilbert transform along k . Here, n is RF sample number, k is sample along the directional signal, and i is emission number. The complex combined signal is [41]

$$\begin{aligned} r_{\text{sq}}(n, k, i) &= x(n, k, i) + j\mathcal{H}_k\{x(n, k, i)\} \\ &= x(n, k, i) + jy(n, k, i). \end{aligned} \quad (4)$$

The received signals are Hilbert transformed in the temporal direction n , and a new directional beamformed signal formed $r_{\text{sqh}}(n, k, i)$ as

$$r_{\text{sqh}}(n, k, i) = \mathcal{H}_n\{x(n, k, i)\} + j\mathcal{H}_n\{y(n, k, i)\}. \quad (5)$$

The signals can be modeled as shown in the equations at the bottom of the page, when assuming monochromatic signals [19], [41]. Here, c is the speed of sound, Δx is the sampling interval along the lateral signal, a is the scattered

amplitude, f_s is the temporal sampling frequency, $\Delta z = c/f_s$, and T_{prf} is the time between pulse emissions. The interrogation depth is d , and the two frequencies received from the axial and lateral motions are given by

$$f_p = \frac{2v_z}{c}f_0 = \frac{2v_z}{\lambda}, \quad f_x = \frac{v_x}{\lambda_x}. \quad (6)$$

Two new signals are then formed from

$$\begin{aligned} r_1(n, k, i) &= r_{\text{sq}}(n, k, i) + jr_{\text{sqh}}(n, k, i) \\ r_2(n, k, i) &= r_{\text{sq}}(n, k, i) - jr_{\text{sqh}}(n, k, i). \end{aligned}$$

The combined signals can be written as

$$\begin{aligned} r_1(n, k, i) &= a \cdot \exp\left(j\frac{2\pi}{\lambda}(2v_z iT_{\text{prf}} - n\Delta z - 2d)\right) \\ &\quad \times \exp\left(j\frac{2\pi}{\lambda_x}(v_x iT_{\text{prf}} - k\Delta x)\right) \end{aligned} \quad (7)$$

and

$$\begin{aligned} r_2(n, k, i) &= a \cdot \exp\left(j\frac{2\pi}{\lambda}(2v_z iT_{\text{prf}} - n\Delta z - 2d)\right) \\ &\quad \times \exp\left(-j\frac{2\pi}{\lambda_x}(v_x iT_{\text{prf}} - k\Delta x)\right). \end{aligned} \quad (8)$$

Both r_1 and r_2 are influenced by the lateral and axial velocities, and this has previously been separated out using the fourth-order autocorrelation estimators derived in [19] and [41]. For a purely lateral velocity, there is no influence from the axial velocity, and the signals can be cross-correlated to find the spatial shift between two emissions and thereby v_x . For other angles, the estimation process will be distorted to not yield the correct v_x . This is, for example, addressed in directional beamforming [42], [43], which noted the same problem with the transverse correlation approach suggested by Bonnefous [44].

The axial velocity component can be removed by multiplying the two signals as suggested by Anderson [45]. This results in the signal

$$\begin{aligned} r_{\text{mult}}(n, k, i) &= r_1^*(n, k, i)r_2(n, k, i) \\ &= a \cdot \exp\left(-j\frac{2\pi}{\lambda}(2v_z iT_{\text{prf}} - n\Delta z - 2d)\right) \\ &\quad \times \exp\left(-j\frac{2\pi}{\lambda_x}(v_x iT_{\text{prf}} - k\Delta x)\right) \\ &\quad \times \exp\left(j\frac{2\pi}{\lambda}(2v_z iT_{\text{prf}} - n\Delta z - 2d)\right) \\ &\quad \times \exp\left(-j\frac{2\pi}{\lambda_x}(v_x iT_{\text{prf}} - k\Delta x)\right), \\ &= a \times \exp\left(-j\frac{4\pi}{\lambda_x}(v_x iT_{\text{prf}} - k\Delta x)\right) \end{aligned} \quad (9)$$

$$\begin{aligned} r_{\text{sq}}(n, k, i) &= a\frac{1}{2} \left(\exp\left(j2\pi \left(\left(\frac{v_x}{\lambda_x} + \frac{2v_z}{\lambda} \right) iT_{\text{prf}} - \frac{k\Delta x}{\lambda_x} - f_0 \frac{n}{f_s} + \frac{2d}{c} f_0 \right) \right) \right. \\ &\quad \left. + \exp\left(j2\pi \left(\left(\frac{v_x}{\lambda_x} - \frac{2v_z}{\lambda} \right) iT_{\text{prf}} - \frac{k\Delta x}{\lambda_x} - f_0 \frac{n}{f_s} + \frac{2d}{c} f_0 \right) \right) \right) \\ r_{\text{sqh}}(n, k, i) &= a\frac{1}{2j} \left(\exp\left(j2\pi \left(\left(\frac{v_x}{\lambda_x} + \frac{2v_z}{\lambda} \right) iT_{\text{prf}} - \frac{k\Delta x}{\lambda_x} - f_0 \frac{n}{f_s} + \frac{2d}{c} f_0 \right) \right) \right. \\ &\quad \left. - \exp\left(j2\pi \left(\left(\frac{v_x}{\lambda_x} - \frac{2v_z}{\lambda} \right) iT_{\text{prf}} - \frac{k\Delta x}{\lambda_x} - f_0 \frac{n}{f_s} + \frac{2d}{c} f_0 \right) \right) \right) \end{aligned}$$

where $r_1^*(\cdot)$ denotes the complex conjugate. The multiplication, thus, removes the influence from the axial velocity, and the resulting signals can be directly correlated to yield the velocity as

$$\begin{aligned} R_{12}(n, m) &= \sum_{i=1}^{N_e} \sum_{k=1}^{N_s} r_{\text{mult}}^*(n, k, i) r_{\text{mult}}(n, k + m, i + 1) \\ &= \sum_{i=1}^{N_e} \sum_{k=1}^{N_s} a \exp\left(j \frac{4\pi}{\lambda_x} (v_x i T_{\text{prf}} - k \Delta x)\right) \\ &\quad a \exp\left(-j \frac{4\pi}{\lambda_x} (v_x (i + 1) T_{\text{prf}} - (k + m) \Delta x)\right) \\ &= a^2 \exp\left(j 2 \frac{4\pi}{\lambda_x} (v_x T_{\text{prf}} - m \Delta x)\right) \end{aligned} \quad (10)$$

where N_e is the number of emissions, and N_s is the number of samples in the directional line. This correlation function has a global maximum for $m_p = v_x T_{\text{prf}} / \Delta x$, when a pulsed signal is used. The maximum can be found from the absolute value of the complex correlation function or from the real part of $R_{12}(n, m)$, where the last method gives the most precise determination. The peak value is found as an integer, which limits the precision. It can be increased by using parabolic interpolation by fitting a second-order polynomial to the three points around the peak value. An interpolated peak value is found in [46]

$$m_{\text{int}} = m_p - \frac{\hat{R}_{12}(m_p + 1) - \hat{R}_{12}(m_p - 1)}{2(\hat{R}_{12}(m_p + 1) - 2\hat{R}_{12}(m_p) + \hat{R}_{12}(m_p - 1))} \quad (11)$$

to yield the interpolated estimate

$$\hat{v}_{\text{int}} = \frac{m_{\text{int}} \Delta x}{T_{\text{prf}}}. \quad (12)$$

Similar expressions can also be found for the axial cross-correlation estimator.

This new estimator has a number of advantages over the autocorrelation approach. Only knowledge of T_{prf} and Δx is needed to get quantitative results. No calibration estimate of $f_x = 1/\lambda_x$, thus, has to be found as in [41]. Furthermore, the velocity range is not restricted to spatial shifts between $-\lambda_x/2$ and $+\lambda_x/2$ as cross-correlation estimators have no inherent aliasing limit, apart from the decorrelation of signals from transverse beam modulation. This can potentially yield a much higher detectable velocity range, with a reduced beamforming load compared to directional beamforming [42], [43]. This estimator design can also be used for making the transverse spectrum as described in [47].

The cross-correlation limit is determined by the time over which two received signals are correlated, which is determined by the width of the PSF compared to the motion $v_x T_{\text{prf}}$. In SAF, the entire focusing is performed during the receive processing, and this can be adapted to the velocity investigated. The lateral oscillation wavelength can be increased by changing the apodization function to have peaks closer to each other on the virtual aperture for high velocities, or they can be separated more to increase the lateral oscillation frequency

for low-velocity estimation. It is also possible to increase the lateral oscillation frequency by using a two-peak apodization in both transmit and receive focusing. An alternative approach is to use full dynamic focusing and then create the lateral oscillation in the frequency domain as suggested in [48] and [49].

V. CONCLUSION

This paper has described two new methods for increasing the maximum detectable velocity of SA velocity imaging using spherical or plane waves. A new sequence design can increase the velocity limit by a factor N equal to the sequence length, and the new TO directional cross-correlation estimator can break the aliasing limit. It also has a higher aliasing limit by a factor 2–4 than for axial autocorrelation estimation, as the lateral wavelength easily can be made two to four times larger than the axial wavelength [18]. The employment of a cross-correlation estimator instead of the autocorrelation approach further adds a factor of 3 as experimentally shown in the accompanying paper [21]. The combination of all these features makes it possible to estimate lateral velocity components $6N$ to $12N$ times higher than for axial velocity components in the previous SA velocity sequences. The approach described in [3] used $N = 8$ and $f_{\text{prf}} = 3$ kHz to estimate peak velocities around 0.15 m/s using directional cross-correlation. The aliasing limit for an autocorrelation system would be 0.04 m/s. The same setup could translate to a peak detectable velocity of 4.6–9.2 m/s using the new scheme and estimator at 3 MHz. Increasing f_{prf} to 5 kHz for full cardiac imaging could lead to velocity range above 10 m/s; enough to detect jets from regurgitation in heart valves.

The interleaved approach is not restricted to use with the new DTO cross-correlation estimator but can be used with any of the current velocity estimators used for axial and vectorial velocity estimations [8], [31] and still attain a factor of N increase in maximum detectable velocity.

The accompanying paper [21] investigates the methods using Field II simulations [22], [23] and measurements from the SARUS experimental scanner [24]. It is demonstrated that velocities of 0.5 m/s can be estimated for an f_{prf} of 450 Hz, which translates to 5.6 m/s at $f_{\text{prf}} = 5$ kHz, and in certain cases at $f_{\text{prf}} = 225$ Hz, a velocity of 0.5 m/s could be estimated corresponding to 11.2 m/s at 5 kHz.

The method still has the advantage of continuous data, and the lowest velocity detectable is, therefore, only limited by the duration over which the data can be acquired for the position in the image. The velocity range, therefore, both cover high velocities in the major arteries, at the same time, as low-velocity flow in small vessels can be estimated from the same data.

REFERENCES

- [1] S. I. Nikolov and J. A. Jensen, "Velocity estimation using synthetic aperture imaging," in *Proc. IEEE Ultrason. Symp.*, Oct. 2001, pp. 1409–1412.
- [2] S. I. Nikolov and J. A. Jensen, "In-vivo synthetic aperture flow imaging in medical ultrasound," *IEEE Trans. Ultrason., Ferroelectr., Freq. Control*, vol. 50, no. 7, pp. 848–856, Jul. 2003.

- [3] J. A. Jensen and S. I. Nikolov, "Directional synthetic aperture flow imaging," *IEEE Trans. Ultrason., Ferroelectr., Freq. Control*, vol. 51, no. 9, pp. 1107–1118, Sep. 2004.
- [4] E. Macé, G. Montaldo, I. Cohen, M. Baulac, M. Fink, and M. Tanter, "Functional ultrasound imaging of the brain," *Nature Methods*, vol. 8, pp. 662–664, Jul. 2011.
- [5] E. Mace, G. Montaldo, B.-F. Osmanski, I. Cohen, M. Fink, and M. Tanter, "Functional ultrasound imaging of the brain: Theory and basic principles," *IEEE Trans. Ultrason., Ferroelectr., Freq. Control*, vol. 60, no. 3, pp. 492–506, Mar. 2013.
- [6] J. A. Jensen, S. I. Nikolov, K. L. Gammelmark, and M. H. Pedersen, "Synthetic aperture ultrasound imaging," *Ultrasonics*, vol. 44, pp. e5–e15, Dec. 2006.
- [7] M. Tanter and M. Fink, "Ultrafast imaging in biomedical ultrasound," *IEEE Trans. Ultrason., Ferroelectr., Freq. Control*, vol. 61, no. 1, pp. 102–119, Jan. 2014.
- [8] J. A. Jensen, S. I. Nikolov, A. C. H. Yu, and D. Garcia, "Ultrasound vector flow imaging—Part II: Parallel systems," *IEEE Trans. Ultrason., Ferroelectr., Freq. Control*, vol. 63, no. 11, pp. 1722–1732, Nov. 2016.
- [9] J. Jensen, M. B. Stuart, and J. A. Jensen, "Optimized plane wave imaging for fast and high-quality ultrasound imaging," *IEEE Trans. Ultrason., Ferroelectr., Freq. Control*, vol. 63, no. 11, pp. 1922–1934, Nov. 2016.
- [10] R. Moshavegh, J. Jensen, C. A. Villagomez-Hoyos, M. B. Stuart, M. C. Hemmsen, and J. A. Jensen, "Optimization of synthetic aperture image quality," *Proc. SPIE*, vol. 9790, pp. 97900Z-1–97900Z-9, Apr. 2016.
- [11] J. A. Jensen, *Estimation of Blood Velocities Using Ultrasound: A Signal Processing Approach*. New York, NY, USA: Cambridge Univ. Press, 1996.
- [12] J. Jensen, C. A. Villagómez-Hoyos, M. B. Stuart, C. Ewertsen, M. B. Nielsen, and J. A. Jensen, "In vivo high frame rate vector flow imaging using plane waves and directional beamforming," in *Proc. IEEE Int. Ultrason. Symp.*, Sep. 2016, pp. 1–4.
- [13] O. Bonnefous, P. Pesqué, and X. Bernard, "A new velocity estimator for color flow mapping," in *Proc. IEEE Ultrason. Symp.*, Nov. 1986, pp. 855–860.
- [14] P. M. Embree and W. D. O'Brien, "The accurate ultrasonic measurement of the volume flow of blood by time domain correlation," in *Proc. IEEE Ultrason. Symp.*, Oct. 1985, pp. 963–966.
- [15] G. E. Trahey, J. W. Allison, and O. T. von Ramm, "Angle independent ultrasonic detection of blood flow," *IEEE Trans. Biomed. Eng.*, vol. BME-34, no. 12, pp. 965–967, Dec. 1987.
- [16] C. Kasai, K. Namekawa, A. Koyano, and R. Omoto, "Real-time two-dimensional blood flow imaging using an autocorrelation technique," *IEEE Trans. Sonics Ultrason.*, vol. 32, no. 3, pp. 458–464, May 1985.
- [17] D. Posada *et al.*, "Staggered multiple-PRF ultrafast color Doppler," *IEEE Trans. Med. Imag.*, vol. 35, no. 6, pp. 1510–1521, Jun. 2016.
- [18] J. A. Jensen and P. Munk, "A new method for estimation of velocity vectors," *IEEE Trans. Ultrason., Ferroelectr., Freq. Control*, vol. 45, no. 3, pp. 837–851, May 1998.
- [19] J. A. Jensen, "A new estimator for vector velocity estimation [medical ultrasonics]," *IEEE Trans. Ultrason., Ferroelectr., Freq. Control*, vol. 48, no. 4, pp. 886–894, Jul. 2001.
- [20] M. E. Anderson, "Multi-dimensional velocity estimation with ultrasound using spatial quadrature," *IEEE Trans. Ultrason., Ferroelectr., Freq. Control*, vol. 45, no. 3, pp. 852–861, May 1998.
- [21] J. A. Jensen, "Estimation of high velocities in synthetic aperture imaging—Part II: Experimental investigation," *IEEE Trans. Ultrason., Ferroelectr., Freq. Control*, vol. 66, no. 6, pp. 1032–1038, Jun. 2019.
- [22] J. A. Jensen and N. B. Svendsen, "Calculation of pressure fields from arbitrarily shaped, apodized, and excited ultrasound transducers," *IEEE Trans. Ultrason., Ferroelectr., Freq. Control*, vol. 39, no. 2, pp. 262–267, Mar. 1992.
- [23] J. A. Jensen, "Field: A program for simulating ultrasound systems," *Med. Biol. Eng. Comput.*, vol. 34, no. 1, pp. 351–352, 1996.
- [24] J. A. Jensen *et al.*, "SARUS: A synthetic aperture real-time ultrasound system," *IEEE Trans. Ultrason., Ferroelectr., Freq. Control*, vol. 60, no. 9, pp. 1838–1852, Sep. 2013.
- [25] S. I. Nikolov, "Synthetic aperture tissue and flow ultrasound imaging," Ph.D. dissertation, Ørsted•DTU, Tech. Univ. Denmark, Lyngby, Denmark, 2001.
- [26] M. Karaman, P.-C. Li, and M. O'Donnell, "Synthetic aperture imaging for small scale systems," *IEEE Trans. Ultrason., Ferroelectr., Freq. Control*, vol. 42, no. 3, pp. 429–442, May 1995.
- [27] C. H. Frazier and W. D. O'Brien, "Synthetic aperture techniques with a virtual source element," *IEEE Trans. Ultrason., Ferroelectr., Freq. Control*, vol. 45, no. 1, pp. 196–207, Jan. 1998.
- [28] K. L. Gammelmark and J. A. Jensen, "Multielement synthetic transmit aperture imaging using temporal encoding," *IEEE Trans. Med. Imag.*, vol. 22, no. 4, pp. 552–563, Apr. 2003.
- [29] C. Demené *et al.*, "Spatiotemporal clutter filtering of ultrafast ultrasound data highly increases Doppler and fUltrasound sensitivity," *IEEE Trans. Med. Imag.*, vol. 34, no. 11, pp. 2271–2285, Nov. 2015.
- [30] C. A. Villagómez-Hoyos, J. Jensen, C. Ewertsen, K. L. Hansen, M. B. Nielsen, and J. A. Jensen, "Energy based clutter filtering for vector flow imaging," in *Proc. IEEE Int. Ultrason. Symp.*, Sep. 2017, pp. 1–4.
- [31] J. A. Jensen, S. I. Nikolov, A. C. H. Yu, and D. Garcia, "Ultrasound vector flow imaging—Part I: Sequential systems," *IEEE Trans. Ultrason., Ferroelectr., Freq. Control*, vol. 63, no. 11, pp. 1704–1721, Nov. 2016.
- [32] S. I. Nikolov, K. Gammelmark, and J. A. Jensen, "Recursive ultrasound imaging," in *Proc. IEEE Ultrason. Symp.*, vol. 2, Oct. 1999, pp. 1621–1625.
- [33] N. Oddershede and J. A. Jensen, "Effects influencing focusing in synthetic aperture vector flow imaging," *IEEE Trans. Ultrason., Ferroelectr., Freq. Control*, vol. 54, no. 9, pp. 1811–1825, Sep. 2007.
- [34] K. L. Gammelmark and J. A. Jensen, "2-D tissue motion compensation of synthetic transmit aperture images," *IEEE Trans. Ultrason., Ferroelectr., Freq. Control*, vol. 61, no. 4, pp. 594–610, Apr. 2014.
- [35] L. A. F. Ledoux, P. J. Brands, and A. P. G. Hoeks, "Reduction of the clutter component in Doppler ultrasound signals based on singular value decomposition: A simulation study," *Ultrason. Imag.*, vol. 19, no. 1, pp. 1–18, 1997.
- [36] S. Bjærum, H. Torp, and K. Kristoffersen, "Clutter filter design for ultrasound color flow imaging," *IEEE Trans. Ultrason., Ferroelectr., Freq. Control*, vol. 49, no. 2, pp. 204–216, Feb. 2002.
- [37] L. Løvstakken, S. Bjærum, K. Kristoffersen, R. Haaverstad, and H. Torp, "Real-time adaptive clutter rejection filtering in color flow imaging using power method iterations," *IEEE Trans. Ultrason., Ferroelectr., Freq. Control*, vol. 53, no. 9, pp. 1597–1608, Sep. 2006.
- [38] A. C. H. Yu and L. Løvstakken, "Eigen-based clutter filter design for ultrasound color flow imaging: A review," *IEEE Trans. Ultrason., Ferroelectr., Freq. Control*, vol. 57, no. 5, pp. 1096–1111, May 2010.
- [39] J. Baranger, B. Arnal, F. Perren, O. Baud, M. Tanter, and C. Demené, "Adaptive spatiotemporal SVD clutter filtering for ultrafast Doppler imaging using similarity of spatial singular vectors," *IEEE Trans. Med. Imag.*, vol. 37, no. 7, pp. 1574–1586, Jul. 2018.
- [40] T. Loupas, J. T. Powers, and R. W. Gill, "An axial velocity estimator for ultrasound blood flow imaging, based on a full evaluation of the Doppler equation by means of a two-dimensional autocorrelation approach," *IEEE Trans. Ultrason., Ferroelectr., Freq. Control*, vol. 42, no. 4, pp. 672–688, Jul. 1995.
- [41] J. A. Jensen, "Directional transverse oscillation vector flow estimation," *IEEE Trans. Ultrason., Ferroelectr., Freq. Control*, vol. 64, no. 8, pp. 1194–1204, Aug. 2017.
- [42] J. A. Jensen, "Directional velocity estimation using focusing along the flow direction—Part I: Theory and simulation," *IEEE Trans. Ultrason., Ferroelectr., Freq. Control*, vol. 50, no. 7, pp. 857–872, Jul. 2003.
- [43] J. A. Jensen and R. Bjerngaard, "Directional velocity estimation using focusing along the flow direction—Part II: Experimental investigation," *IEEE Trans. Ultrason., Ferroelectr., Freq. Control*, vol. 50, no. 7, pp. 873–880, Jul. 2003.
- [44] O. Bonnefous, "Measurement of the complete (3D) velocity vector of blood flows," in *Proc. IEEE Ultrason. Symp.*, Oct. 1988, pp. 795–799.
- [45] M. E. Anderson, "A heterodyning demodulation technique for spatial quadrature," in *Proc. IEEE Ultrason. Symp.*, Oct. 2000, pp. 1487–1490.
- [46] S. G. Foster, "A pulsed ultrasonic flowmeter employing time domain methods," Ph.D. dissertation, Dept. Elect. Eng., Univ. Illinois Urbana-Champaign, Champaign, IL, USA, 1985.
- [47] J. A. Jensen, "Transverse spectral velocity estimation," *IEEE Trans. Ultrason., Ferroelectr., Freq. Control*, vol. 61, no. 11, pp. 1815–1823, Nov. 2014.
- [48] H. Liebgott, "Fourier domain beamforming for transverse-oscillations," in *Proc. IEEE Int. Ultrason. Symp.*, Oct. 2010, pp. 1755–1758.
- [49] M. Lenge, A. Ramalli, P. Tortoli, C. Cachard, and H. Liebgott, "Plane-wave transverse oscillation for high-frame-rate 2-D vector flow imaging," *IEEE Trans. Ultrason., Ferroelectr., Freq. Control*, vol. 62, no. 12, pp. 2126–2137, Dec. 2015.



Jørgen Arendt Jensen (M'93–SM'02–F'12) received the M.Sc., Ph.D., and Dr.Techn. degrees from the Technical University of Denmark in 1985, 1989, and 1996, respectively.

In 2003, he was one of the founders of the Biomedical Engineering Program in medicine and technology, which is a joint degree program between the Technical University of Denmark and the Faculty of Health and Medical Sciences at the University of Copenhagen, Copenhagen, Denmark.

The degree is one of the most sought-after engineering degrees in Denmark. He was the Chairman of the study board, from 2003 to 2010. He was an Adjunct Professor with the University of Copenhagen, from 2005 to 2010. He was the Founder and the Head of the Biomedical Engineering Group, Technical University of Denmark, from 2007 to 2010. Since 1993, he has been a Full Professor of biomedical signal processing with the Department of Electrical Engineering, Technical University of Denmark, Kongens Lyngby, Denmark. He has been the Founder and the Head of the Center for Fast Ultrasound Imaging (CFU), Kongens Lyngby, since its inauguration in 1998. CFU has contributed with innovations

in transverse oscillation vector flow imaging, synthetic aperture flow imaging in 2-D and 3-D, ultrasound simulation, research scanners, and row-column probes and beamforming. He is currently the Developer and Maintainer of the Field II Simulation Program. He has been a Visiting Scientist at Duke University, Durham, NC, USA; Stanford University, Stanford, CA, USA; and the University of Illinois at Urbana–Champaign, IL, USA. He has authored or coauthored more than 450 journal and conference papers on signal processing and medical ultrasound, and the book *Estimation of Blood Velocities Using Ultrasound* (Cambridge University Press, 1996). He has given a number of short courses on simulation, synthetic-aperture imaging, and flow estimation at international scientific conferences and teaches biomedical signal processing and medical imaging at the Technical University of Denmark. His research is centered around the simulation of ultrasound imaging, synthetic-aperture imaging, vector blood flow estimation, 3-D imaging, row-column probes, and construction of ultrasound research systems.

Dr. Jensen has given more than 60 invited talks at international meetings and received several awards for his research, most recently the Grand Solutions Prize from the Danish Minister of Science and the order of the Dannebrog by her Majesty the Queen of Denmark.